Myocardial Strain Analysis and Heart Rate Variability as Measures of Cardiomyopathy in Duchenne Muscular Dystrophy

By

John Ernesto Mendoza

Thesis

Submitted to the Faculty of the
Graduate School of Vanderbilt University
in partial fulfillment of the requirements
for the degree of

MASTER OF SCIENCE
in
Biomedical Engineering

May, 2017
Nashville, Tennessee, USA

Approved:

Bruce M. Damon, Ph.D.
Jonathan H. Soslow, M.D.

ACKNOWLEDGEMENTS

I would like to thank the Vanderbilt University Institute of Imaging Science and the Vanderbilt University Department of Biomedical Engineering for their continuous support. Also, I would like to thank the Vanderbilt University Children's Hospital, Department of Pediatrics, Division of Cardiology for their cooperation and the Vanderbilt Institute for Clinical and Translational Research grant support from the NCATS and the NIH. Thank you to Dr. Larry W. Markham, Associate Professor of Pediatrics, for his guidance and clinical expertise. I would like to especially thank Dr. Jonathan H. Soslow, Assistant Professor of Pediatrics, for not only allowing us to work with his clinical data, but also for his continuous support and cooperation throughout our investigation.

I am very grateful for the members of the VUIIS Muscle Physiology Lab who have helped me along the way. Thank you to Dr. Crystal Coolbaugh, Postdoctoral Research Fellow, and Dr. Amanda Buck, Instructor in Biomedical Engineering, for supporting me throughout my research and helping me persevere through challenging obstacles. Perhaps the greatest factor in my success has been my PI, Dr. Bruce M. Damon, who has never failed to encourage me to always perform to my greatest ability and has truly inspired me to make a difference with what I have learned at Vanderbilt University.

Lastly, I would like to thank my family and friends who have always been there to make sure I never felt alone. Their love and care has been the fuel for all of this work and I am proud to be a simple example of their unending support.

TABLE OF CONTENTS

LIST OF TABLES

LIST OF FIGURES

Chapter 1: Introduction

DMD Epidemiology & Pathophysiology

Duchenne Muscular Dystrophy (DMD) is a recessive X-linked myopathy that arises from mutations in the gene that encodes the protein dystrophin. The progressive, degenerative myopathy is characterized largely by muscle weakness and atrophy due to reduced or, more commonly, an absence of dystrophin production.

DMD occurs once in approximately every 3500 live male births, making it the most common inherited pediatric muscle disorder. Spontaneous mutations in the dystrophin gene, most of which are deletions, lead directly to either a deficiency of dystrophin or the synthesis of a functionally impotent version of the protein. Dystrophin is a sarcolemmal protein and is a critical component of the dystrophin glycoprotein complex (DGC), also known as the dystrophin-associated protein complex (DAPC). This protein complex acts to anchor the intracellular cytoskeleton with the extracellular matrix in contractile muscle cells.[1,2] The dysfunction of this protein complex across the cell membrane induces transient local membrane disruptions and leakage, leading to an abnormal flow of calcium ions into the cell due to the strong concentration gradient that exists across the membrane. Studies have shown that calcium concentrations in dystrophic muscle are higher than in healthy muscle.[3] This abnormal calcium homeostasis has been observed in muscle fibers, sarcoplasmic reticula, and in sub-sarcolemmal free calcium count in DMD patients.[3] This influx activates calcium-dependent proteases within the cell that further alter calcium channel activity, thus creating a pathological positive feedback system. The inability for a myocyte to regulate its calcium levels inevitably leads to contraction-induced damage, inflammation, and necrosis.[4]

Early disease signs may include mildly delayed motor milestones; some individuals are unable to run or jump due to the effects on skeletal muscle. Most boys are diagnosed at approximately 5 years of age when the motor inability of affected individuals diverges heavily from healthy young boys. Furthermore, most patients lose independent ambulation by age 13.[5,6] Becker muscular dystrophy (BMD) is a milder form of the disease that has both a later onset and longer survival, though it is characterized by a dystrophin deficiency rather than an absence. In DMD, the patients first experience early weakness in proximal lower limbs muscles, followed by shoulder muscles, distal limb muscles, respiratory-related skeletal muscles, and eventually cardiac tissue.[7] DMD patients also experience autonomic dysfunction at relatively young ages, which has been recently suggested to be the driving force for various cardiac complications later in life.[8] A weakened heart brought about by cardiomyopathy, as seen in DMD, initiates a compensatory phenomenon in the body. Sympathetic input to the heart, combined with withdrawal of parasympathetic input, increases cardiac output and aids a diseased heart by complementing the work required. However, the inability to provide sufficient autonomic compensation would lead to a greater onset of cardiac complications and heart failure, prompting targeted heart failure therapy.

DMD Therapy Frontier

Though there is no established therapy for DMD, there exist promising techniques aimed to treat or cure the disease. Gene therapy looks to restore the functional capacity of contractile cells by delivering a synthetic copy of the dystrophin gene to affected nuclei in muscle fibers. One challenge that presented itself early on was the difficulty in developing a delivery mechanism that could encapsulate the large dystrophin cDNA sequence (13 kb).[1] In response, researchers have developed micro-dystrophin sequences that are designed to repair the specific sequence deletions

commonly observed within the affected dystrophin gene. The use of retroviruses, lentiviruses, and adenoviruses have shown promise in delivering these synthetic dystrophin genes into muscle cells and increasing trans-gene expression and regenerative abilities in young animal models.[9] However, the immunogenicity of these viral vectors introduce a risk of adverse systemic immune responses to treatment, thus limiting their use until immunocompatible methods are developed. Non-viral delivery techniques, including unencapsidated plasmids and genome-editing strategies, are also being developed to introduce dystrophin cDNA into affected nuclei.[10] Stem cell therapies are also being heavily investigated as a means of restoring the production of dystrophin with new, healthy nuclei in myocytes. The transplantation of both satellite stem cells and bone marrow- / muscle-derived stem cells to treat muscular dystrophy has been gaining attention in recent years. The use of autologous or allogenic stem cell transfers has the potential of providing self-renewing and long-lasting treatment.[10,11] Still, current treatment options are limited to pharmacological intervention, including the use of glucocorticoid corticosteroids such as prednisone and deflazacort, which have been shown to lead to an improvement in muscle strength and function.[5,6,12,13] However, there is increasing concern regarding side effects of these commonly used steroids on boys with DMD.[13] Though emerging steroid treatments, such as eplerenone and vamorolone, have shown promising improved results in treating DMD[14,15], care providers still rely extensively on disease monitoring and pharmacological intervention aimed to improve patient quality of life and to increase life expectancy.

Hands-on orthopedic and neuromuscular management usually begin prior to early non-ambulatory stages of the disease. This includes biannual assessments of function, strength, and range of movement, which help define the pharmacological regimen of interventional agents like glucocorticoids. Once the patient has begun to lose independence with their daily activities, the

monitoring of spinal complications, such as scoliosis or podiatric complications (e.g. foot repositioning), is introduced.[5,6] However, the improvements in the comprehensive therapeutic approaches for pulmonary and cardiac complications are what have made the largest impact on DMD life expectancy.

Without intervention, the life expectancy in patients with DMD is approximately 19 years; pulmonary and cardiac therapies have lengthened the life expectancy of DMD patients diagnosed today into the fourth decade of life.[16,17] Regarding pulmonary pharmacological interventions, corticosteroids and idebenone have been used to significantly reduce the decline of spirometric (pulmonary system-related) parameters associated with the disease. Furthermore, lung volume recruitment techniques, also known as "breath stacking", have been used to reduce the risk of atelectasis, or lung collapse, and slow the rate of decline of lung function. In later stages of the disease, scoliosis steroid therapy aimed to reduce muscle inflammation and degeneration is used to reduce the restrictive pulmonary effects that result from the spinal complication. Cost-assisted devices improve airway clearance and reduce the risk of infections such as pneumonia. Lastly, non-invasive mechanical ventilation techniques are used to improve respiratory function during sleep to prevent nocturnal adverse events, which could induce respiratory failure.[7] Due to these advancements in respiratory support and the subsequent longer life expectancy, cardiac complications and heart failure have become the leading causes of death in patients with DMD, prompting a great need for cardiac management and cardiomyopathy tracking.[18]

Cardiomyopathy Associated with DMD

While the exact onset of cardiomyopathy varies considerably between patients, cardiac complications are usually pervasive across the childhood of a DMD patient.[19] Early on, diastolic dysfunction and focal fibrosis can occur in the heart; this proceeds to dilated cardiomyopathy

(DCM) and is almost always complicated by arrhythmia and heart failure. In late stage DMD, occurring in late second decade or third decade, cardiac arrhythmias resemble those in other cardiomyopathies such as atrial/ventricular fibrillation and ventricular tachycardia. Arrhythmia complications are identified as a potentially major contributor to DMD mortality, though this still requires heavy investigation.[20] In general, cardiomyopathy associated with DMD is characterized by a normal or thinning left ventricular (LV) wall with progressive decline in LV ejection fraction (LVEF). The exact mechanisms of this pathophysiology are still under investigation, limiting current treatments to remain untargeted and streamlined. One hypothesis for the cause of the cardiomyopathy is that the structural integrity of cardiomyocytes is severely compromised due to the lack of dystrophin in the DGC. The hemodynamic stress occurring during normal LV function would then give rise to tissue damage and deterioration. Another hypothesis proposes that dystrophin and the DGC play a role in protein regulation.

Investigating alternative pharmacological interactions, such as with nitric oxide production and transforming growth factor-β (TFGβ), has shown promise for a source of targeted pharmacological therapy.[21] Also, glucocorticoid steroid therapy has been shown to alter the progressive decline in cardiac function in DMD patients.[22] Yet it still remains that angiotensin-converting enzyme (ACE) inhibitors and β-adrenoceptor blockers, or β-blockers, are two more commonly used medications aimed at specifically treating cardiac dysfunction. The use of ACE inhibitors is well-established to prevent pathologic LV remodeling, dilation, and systolic dysfunction.21[21] Previous uses of ACE inhibitors in studies with young patients with DMD have shown a significant increase in survival rate when ACE inhibitors were used as a prophylactic treatment to delay or prevent DCM in DMD.[23] Though the use of β-blockers is less well-established when compared to ACE inhibitors, its use for nonsyndromic asymptomatic cardiac

dysfunction has shown success in DMD patients. For example, one study showed higher rates of survival and heart failure-free survival when a patient with DMD received β-blockers.[24] By reducing sympathetic tone, β-blockers work to normalize autonomic regulation of the heart; again, this effect has been shown to significantly reduce cardiac-related mortality.[25] It is important to note that β-blocker treatments have been shown to lower heart rate (HR), which would affect characterization of DMD patients' HR patterns.[26] These two medications are not used exclusively; one study showed that an ACE inhibitor alone or in combination with a β-blocker showed improvement in LV ejection fraction.[27] Regardless, the use of ACE inhibitors remains the first-line therapy once LV dysfunction has developed.[20] Clinical guidelines suggest evaluations should be performed every two years after disease diagnosis and yearly after ten years of age.[21] In order to diagnose and characterize the disease at each evaluation, highly sensitive monitoring/detection techniques are needed to deliver optimized treatment.

Assessing Cardiomyopathy Using Medical Imaging

Early detection of cardiomyopathy in DMD patients is critical as early protective measures can lead to improved cardiac function in later stages of the disease. One study has recently proposed a significant relationship between cardiac and skeletal muscle dysfunction in non-ambulatory DMD patients; this suggests that sensitive monitoring of cardiac function is imperative, even when quantities of interest are not cardiac-related.[28] Traditionally, clinicians have used transthoracic echocardiography (TTE) to measure LVEF to characterize the extent of the cardiomyopathy.[29, 30] This modality, however, has practical challenges in the DMD patient population as TTE rarely detected cardiac defects in the patient's first decade. Furthermore, the modality struggled with small acoustic windows due to DMD complications including scoliosis and chest wall adiposity.[31, 32] Additionally, although cardiomyopathy is classically defined as

having an LVEF <55%, a reduced LVEF occurs only after significant myocardial damage and is, therefore, often a late finding in DMD.[33]

Alternatively, cardiovascular magnetic resonance (CMR) has proven to be a more sensitive detection modality for cardiomyopathy in patients with DMD. One study showed that when using CMR, researchers were able to detect myocardial fibrosis in patients where other modalities were unable to do so during a standard cardiac evaluation.[3333] Another study supported this claim by showing that CMR was able to detect early myocardial scarring before LVEF was significantly affected by the disease.[34] Furthermore, it has also been shown that TTE measurements show poor correlation with CMR data and introduce unrecognized LV wall motion abnormalities which could negatively impact patient quality of care.[35]

An alternative metric used to characterize DMD cardiomyopathy is quantifying LV wall strain. One study demonstrated that in muscular dystrophies, CMR data revealed subtle abnormalities in systolic circumferential strain in the LV while there was still no detectable fibrosis.[36] In fact, myocardial strain analysis has become a well-trusted method of characterizing early cardiomyopathy in patients with DMD. One study was able to use myocardial strain analysis to detect strain abnormalities in patients who still exhibited normal LVEF.[32] This study also showed that when used in combination with standard CMR and myocardial delayed enhancement (MDE), this strain analysis produced specific, stratified cardiomyopathy characterization in patients with DMD.[32]

Myocardial Strain Analysis using Spatial Modulation of Magnetization

It is believed that if therapy can be initiated at an early stage of the disease by using CMR as a screening tool, late stage cardiac dysfunction can be attenuated, though not prevented. This would translate to therapy being administered prior to systolic dysfunction and DCM. In the late

1980s, researchers fully developed a method of MR tagging called spatial modulation of magnetization (SPAMM) that provided a method of tracking motion in moving tissue. In 1989, Axel et al. used SPAMM to measure LV wall motion throughout the cardiac cycle.[37] Since then, SPAMM has become a clinically-used modality that allows clinicians and researchers to measure heart wall motion and, therefore, quantify tissue strain.

Simple SPAMM sequences contain three main components: RF tipping pulses, spatial/tagging gradients, and spoiler gradients. RF tipping pulses applied while using spatial gradients vary the magnitude of the longitudinal magnetization of atomic spins sinusoidally with respect to position. The subsequent spoiler gradient acts to remove any transverse magnetization signal from the image. This sequence produces MR images with an orthogonal grid pattern overlaying the image where each grid line represents areas where signal was significantly diminished while areas between grid lines correspond to areas of high signal. If multiple images are acquired throughout the cardiac cycle, the grid lines can be seen to deform in a manner reflecting the movement of the imaged tissue. These grid lines act as markers by providing each pixel with a phase value corresponding to its position within the sinusoidally-varying magnetization. Strain calculations can then be made by tracking these markers and using their displacement information.

Other methods of quantifying myocardial strain include both cine phase contrast (cine PC) imaging and strain-encoded (SENC) magnetic resonance imaging. Studies qualitatively and quantitatively compared these modalities have shown that SPAMM imaging produces similar results.[38,39]

SPAMM tagging has been proven to be a successful modality to diagnose regional cardiac dysfunction associated with DMD. Researchers have shown that abnormal global and segmental

circumferential strain values can be detected in boys with DMD who have similar LV volumes and LVEF to age- and gender-matched controls.[40] A few years later, another study showed similar findings, concluding that DMD patients with normal LVEF had reduced peak circumferential strain (ε_{cc}) at an early age compared to controls. Researchers also observed that ε_{cc} was further reduced in older patients (>10 years) with normal EF, and even further reduced in older patients with reduced LVEF; the oldest patients, who exhibited reduced LVEF and positive indicators for myocardial fibrosis, had the lowest ε_{cc}.[3232] A third study concluded similar findings in boys with DMD; they found that ε_{cc} abnormalities progressed during periods where LVEF abnormalities were not significant.[41] These studies above suggest that ε_{cc} measurements may provide a reliable, sensitive method of monitoring cardiomyopathy progression in patients with DMD, prior to the development of more serious cardiac complications or even heart failure. However, SPAMM techniques require sophisticated software to extract quantitative parameters from images, including strain.[42]

Harmonic Phase Analysis for Myocardial Strain Quantification

Harmonic phase analysis (HARP) was developed in the late 1990s by Osman et al.[43] This group has published multiple studies showing its utility in extracting quantitative spatial parameters from SPAMM images and using them to calculate myocardial Lagrangian strain.

HARP can be used to extract spatial/displacement measurements from tagged MR images.[43,44,45] Once a SPAMM sequence is performed, a Fourier transform of a single dynamic produces a mapping of the spectral peaks of the MR image. These spectral peaks each correspond to directionally-specific phase information at particular frequencies. By isolating the signal of a single Fourier peak and performing an inverse Fourier transform on the filtered image, the process produces a complex image where the calculated angle is called a HARP image. After further

processing is performed on the HARP image, Osman et al. shares a method of point tracking using these phase markers in order to extract movement parameters from the image.[43] However, there are some practical challenges that arise from using this pixel tracking methodology, such as image registration difficulties due to LV dilation during the cardiac cycle, and artifacts stemming from aliasing pixel positioning. In order to overcome these challenges, we have introduced another method of interpreting HARP images that has been shown to produce accurate strain quantification without using a pixel/fiducial tracking method.

Bayly et al. describes a "gradient-based" analysis that utilizes the prior work done by Osman et al.[46] Osman et al. showed that an apparent deformation gradient tensor can be constructed using processed HARP images. This gradient tensor is comprised of the X- and Y-directional derivatives, or gradients, of the HARP images corresponding to the X- and Y-directional spectral peaks of the Fourier transform of the original SPAMM image.[44] Bayly et al. eliminates the need for a pixel tracking algorithm by introducing a mathematical relationship that uses the undeformed tagging grid's spatial frequency as a reference parameter for each SPAMM image acquired in the cardiac cycle. In other words, rather than requiring an image registration approach where Eulerian strain is calculated by using the undeformed image as a reference image, this algorithm allows researchers to extract 2D displacement and strain values by comparing the deforming SPAMM grid patterns to parameters of the undeformed grid. Though Bayly et al. first utilized this method in quantifying strain in traumatic brain injury models[46], we believe that this approach can be readily applied to accurately quantifying LV Lagrangian strain in patients with DMD.

Heart Rate Variability in DMD

An additional metric we investigated within patients with DMD was heart rate variability (HRV) data. HRV analysis is a non-invasive technique that quantifies fluctuations in heart rate (HR) that occur naturally due to varied systemic/metabolic demands. For decades, it has been well-established that changes in autonomic innervation to the heart can be a hallmark of cardiovascular complications, including heart failure.[47] Since its clinical importance became apparent in the 1980s, clinicians and researchers have sought to use it as a predictor or indicator for various cardiomyopathies. HRV measurements have been well established as a diagnostic tool to patients with DMD as well. In most studies, HRV is generally quantified as a single generalized metric by using various parameters and statistics acquired by either electrocardiogram (ECG) data or RR-interval data; these statistics include both time domain metrics as well as frequency domain values. Historically, "less" heart rate variability in a patient is a sign that the cardiomyopathy of interest is at a more advanced stage.[48,49] However, in order to take full advantage of the specificity of utilizing HRV and how it applies to patients with DMD, we must dissect cardiac monitoring signals and define what a parameter of interest represents physiologically.

Spontaneous and rhythmic depolarizations in the sino-atrial node of the heart determine HR. The frequency of these depolarizations is, however, largely impacted by the parasympathetic and sympathetic divisions of the autonomic nervous system (ANS), each with opposing effects on the heart. The vagus nerve provides parasympathetic innervation to the sinus and atrioventricular nodes as well as the atrial myocardium. By inhibiting the release of sympathetic neurotransmitter and promoting acetylcholine release, vagal stimulation tends to decrease HR and myocardial conduction/contractility.[50] Sympathetic innervation accelerates HR via epinephrine or norepinephrine release. A stable physiological state would include some tonicity from both

sympathetic and parasympathetic systems which would allow for rapid control of HR. However, it has been shown that both an increase in sympathetic activity and a decrease in parasympathetic activity are associated with cardiac complications, including ventricular arrhythmias.[51] In order to determine if this abnormal behavior is present in DMD patients, we can use HRV analysis software to quantify each systems' contribution to the heart by isolating different frequencies within HR power spectrum.[52]

When an individual is at rest, parasympathetic effects dominate the sympathetic effects on HR. Each of these innervations vary regarding the speed at which their effects are realized in the heart. Parasympathetic activity affects the heart more so on a beat-to-beat basis, while sympathetic innervation requires seconds in order for it to achieve peak effects. Also, it has been shown that parasympathetic innervation greatly dominates the high frequency (HF) components of the HR power spectrum, due to the very short latency periods associated with parasympathetic stimulation.[53,54] These high-frequency components of HRV correspond to the modulation of vagal tone. These modulations, which are also linked to respiration, cause short-term alterations of the cycle length of the sinus rhythm.[54] Furthermore, it is understood that sympathetic activity is associated with reduced parasympathetic activity; the two systems act in a complementary, competitive fashion.[55] Note that in order to achieve a true measure of the disease state in patients with DMD, the effects of β-blockers on HRV must be taken in account. Various studies have shown that there exists a measurable difference in heart rate and cardiac function when using β-blockers.[56,57] Though this is the intended effect of the treatment, it would introduce unwanted effect variables into the HRV analysis.

Using the above information we look to quantify the extent of cardiac complications in patients with DMD by using the following reasoning. By performing power spectral analysis on

HR data, we can measure how great the HF component is of any signal, which would provide a measure of parasympathetic innervation.[50] The level of parasympathetic activity would then provide another measure of sympathetic activity, due to their complementary relationship. Therefore, a reduction in the power associated with the HF of a HR signal would reflect reduced parasympathetic input, increased sympathetic input, and an increase in the likelihood of cardiac complications associated with DMD, including ventricular arrhythmias. Overall, if we acquire RR interval data from patients with DMD, and dissect it using established parameters and standards optimized for HRV analysis, we could potentially provide an additional measure of disease progression or severity.[47]

Study Significance on Duchenne Muscular Dystrophy.

This study assessed the viability of using a custom strain analysis method to evaluate cardiomyopathy in patients with DMD. This method combines the deformation gradient tensor construction from Osman et al. with the "gradient-based" analysis by Bayly et al., the latter of which was previously performed only on deformation in mild traumatic brain injuries. Furthermore, this study also assesses the autonomic contribution and effects on HR data and characterizes the relationship between HRV and LV strain. We hypothesized that 1) the combination strain analysis technique developed would be correlated with the results achieved using commercialized HARP software, and 2) that the results seen would be significantly correlated with HRV parameters. The validation of this HARP method could introduce an alternate technique to quantify Lagrangian LV strain in both healthy and diseased subjects. Regarding patients with DMD, this method has the potential to detect previously unseen cardiomyopathic manifestations, which could potentially aid in the development of optimized pharmacological management strategies and move towards a more optimized patient care regimen. A significant

correlation between the measured strain and the HRV parameters would strengthen the argument that HR data or ECG data can be used to predict clinically relevant sequelae without the use of resource-intensive imaging techniques. Furthermore, imaging acquisition sessions can pose both physical and psychological stress on young boys with DMD; providing an alternate, dependable, low-profile form of characterizing cardiomyopathy would contribute to overall patient quality of life. With additional investigation in the future, this research has the potential to directly impact lives of patients suffering from DMD.

Chapter 2: Methods

This IRB-approved study was performed retrospectively on data acquired in Vanderbilt University Medical Center, Department of Pediatrics, Division of Cardiology. Informed assent and consent were obtained before patient participation. 28 boys with DMD were studied (ages 8-21), six of whom were taking β-blockers at the time of the study. The patient population's height (112cm-180cm) and weight (22kg-103kg) ranged significantly. The patients' physical abilities also ranged from patients who were still ambulatory to those who were wheelchair-bound. Inclusion criteria were defined as: 1) 8-25 years old, 2) able to undergo CMR without sedation/anesthesia, and 3) clinical phenotype of DMD confirmed with muscle biopsy or genotype. Exclusion criteria were defined as: 1) refusal to participate, 2) renal dysfunction or other contraindication to MRI with contrast, and 3) diagnosis of other genetic abnormality in addition to DMD.

SPAMM Acquisition

Cardiac MRI data included SPAMM-tagged images, acquired throughout the cardiac cycle, and balanced steady-state free precession (bSSFP) cine images in a short axis stack (latter used for quantification of LVEF). All scans were performed on a 1.5T Siemens Avanto MR imager with an eight-channel cardiac array receiver coil. Each scan lasted between 45-60 minutes and did not include contrast agent injections that affected the SPAMM acquisition. Each patient had at least one sequence of apical, midventricular, and basal short-axis SPAMM-tagged images taken. All analyses were performed on the

Figure 1. SPAMM-tagged image. Short-axis oblique slice through chest of DMD patient.

midsection slice, as this slice has been reported to produce the most reliable circumferential strain results.[40,58] The number of images acquired within each cardiac cycle varied from 5-13 images. An 8 millimeter-spaced orthogonal tagging pattern was used in each SPAMM image, as seen in Figure 1. These images were exported as WinImage IMA files and loaded in MATLAB® to perform HARP and strain analysis.

HARP Analysis

HARP analysis allows us to extract spatial parameters from each SPAMM-tagged image by isolating the phase information with respect to both the X and Y direction. Each SPAMM image was rotated 45 degrees counterclockwise to align the grid pattern in the horizontal (X) and vertical (Y) direction. Each image was also cropped to a 110x110 pixel image centered about the LV. Cropping the image reduced the level of noise and artifacts that arose from the extraneous signal outside of the LV. After preprocessing, a fast Fourier transform was taken to reveal the spectral peaks of the SPAMM image. Each of these peaks represents a harmonic component of the signal in the processed SPAMM image. By constructing a small region of interest (ROI) filter and centering it on the first harmonic X-directional or Y-directional peaks, as seen in Figure 2a, the image's X-directional or Y-directional phase information was isolated. Optimized filter

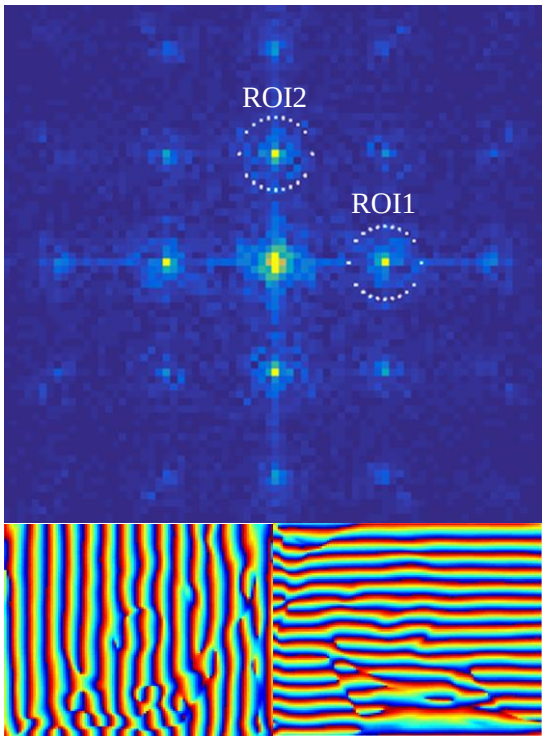

Figure 2. Isolating the phase angle from SPAMM image using fast Fourier transform. The fast Fourier transform of the processed SPAMM-tagged image with circular filters centered on the spectral peaks of interest (top). The X-directional phase angle data constructed by using ROI1 (bottom, left). The Y-directional phase angle data constructed by using ROI2 (bottom, right).

parameters are often debated. These parameters include the 2D spatial dimensions of the filter, as well as the roll-off characteristics at the edge of the filter. Since there are other sources of randomness to the strain result within and between patients, measuring these parameters' impact using an iterative trial-and-error method is neither practical nor effective. Applying a general linear model (GLM) using mixed-effect analysis allowed for comparison of the effects of filter radius (R_f) on the strain values produced by the algorithm. R_f was varied from 3 to 7 pixels with a step size of one-tenth pixel; HARP analysis was performed on 17 SPAMM-tagged image sequences (one per patient available) for each R_f value. This process was performed twice to assure there was no bias in the strain measurements within the GLM algorithm. Additionally, each patient's LVEF and age recorded at the time of SPAMM acquisition were included in the design matrix. A Q-Q plot was used to assess the distribution of the response variables. Of the distribution options for general linear model analysis in MATLAB (i.e. normal, binomial, poisson, gamma, inverse gaussian), a normal distribution had the best fit for the data. See Results section for determination of R_f effect on strain calculations. The filter used for strain calculations exhibited a Gaussian roll-off pattern represented by Equation 1.

$$R_G(p) = \alpha e^{\frac{p^2}{2\gamma^2}} \qquad \text{[Eq. 1]}$$

p represents the pixel length from the edge of the filter. The radius range and parameters $\alpha = 1$ and $\gamma = 2$ were chosen to encompass spectral data corresponding to a maximum ~30% strain magnitude.

Measuring the angle of the reverse fast Fourier transform of the segmented first harmonic spectral peak produces a wrapped HARP image as seen in the bottom of Figure 2. The pixel magnitude in these images range within +/- *pi* and correspond to the angle of the phase of the sinusoidally varying grid tags applied in both the X- and Y- direction. Using the built-in MATLAB

function `roipoly`, an inner ROI of the LV wall was drawn for each SPAMM image within each sequence, as shown in Figure 3. These ROIs exclude signal from LV chamber lining, papillary muscles, and the epicardium.

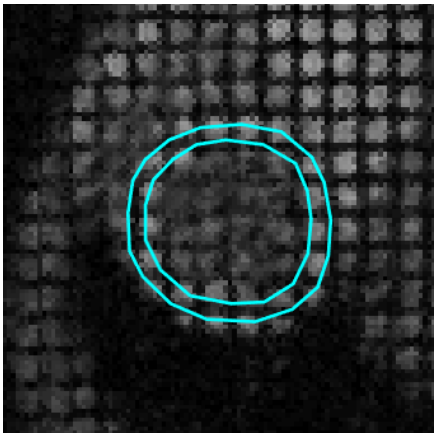

Figure 3. LV ROI example.

An unwrapping algorithm adapted from an open source MATLAB code was then implemented to construct a phase angle gradient from each of the wrapped HARP images produced.[59] Strain analysis depends on each pixel containing a unique unidirectional phase value in order for displacements to be measured. By using this unwrapping algorithm, these unique phase values can be assigned for each pixel in both the X and Y directions. These unwrapped HARP images, seen in Figure 4, represent the main product of HARP analysis.

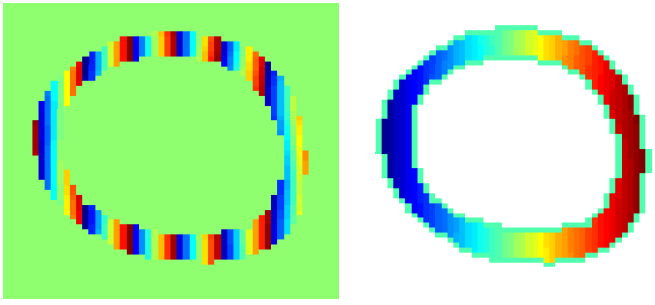

Figure 4. Effects of unwrapping algorithm. Wrapped (left) and unwrapped (right) image.

Strain Analysis

The built-in MATLAB `gradient` function was used to calculate the first derivative of the unwrapped HARP images with respect to both the X and Y directions. These derivatives are the elements of a 2x2 phase vector array defined as in Equation 2.

$$\nabla\varphi(i,j) = \begin{pmatrix} PX_X(i,j) & PX_Y(i,j) \\ PY_X(i,j) & PY_Y(i,j) \end{pmatrix} \qquad \text{[Eq. 2]}$$

$PA_B(i,j)$ represents the gradient, or first derivative, of the *A*-directional unwrapped HARP image with respect to the *B* direction in the pixel in the i^{th} row and j^{th} column. This pixel-specific phase

vector array can be used to calculate the deformation gradient tensor for each pixel in any SPAMM-tagged image, using Equation 3.

$$F(i,j) \cong \nabla\varphi(i,j)^{-1}W^T \qquad \text{[Eq. 3]}$$

$W = [w_x, w_y]$ and w_j is the spatial frequency vector corresponding to the two spectral peaks filtered above. Alternatively, W can be calculated using Equation 4.

$$W = \begin{pmatrix} \frac{2\pi}{s_x} & 0 \\ 0 & \frac{2\pi}{s_y} \end{pmatrix} \qquad \text{[Eq. 4]}$$

$s_x = S/V$ where S is the 8 millimeter tag spacing and V is the voxel size in millimeters. This gradient-based analysis allows us to then calculate a strain tensor *E* using Equation 5.

$$E = (F^T F - I)/2 \qquad \text{[Eq. 5]}$$

F is the constructed deformation gradient tensor and *I* is a 2x2 identity matrix. Diagonalizing the strain tensor for each pixel within the LV provides principal eigenvectors associated with a positive Lagrangian radial strain and a negative Lagrangian circumferential strain in the pixel, the latter of which was used as the primary measure for strain characterization due to its clinical prevalence. After separating the LV wall into 6 segments (anterior, anteroseptal, inferoseptal, inferior, inferolateral, anterolateral), the above analysis was repeated beginning with $PA_B(N)$ gradient values, or the average $PA_B(i,j)$ across all pixels within each segment. This analysis was performed for each image in each SPAMM sequence. The average global circumferential strain (ε_{cc}) was calculated for each SPAMM image in the cardiac cycle. The peak ε_{cc}, occurring during peak systole, was used as our main metric of cardiomyopathy severity, as it is commonly used in clinical diagnoses of DMD cardiac complications. In order to validate the above algorithm, the peak ε_{cc} calculated was directly compared to the peak global Eulerian circumferential strain, acquired using clinically trusted software, in each patient (n=28) using a Pearson correlation and regression

analysis. The small coordinate scaling within the dimensions of the LV wall allowed for a direct correlation between Lagrangian and Eulerian models of circumferential strain.

Heart Rate Variability Analysis

Following cardiac MR acquisition, each patient underwent 48-hour Holter monitoring to record beat-to-beat RR interval data. Holter data were exported into Microsoft Excel 2013 where the RR intervals (in milliseconds) were extracted and saved as text (.txt) files. All .txt files were then loaded into Kubios HRV v2.1 to perform HRV analysis. Kubios HRV is able to analyze specifiable samples of RR interval data to produce both time-domain and frequency-domain outputs, the latter of which was used as a primary measure of autonomic functionality. RR interval data was sampled according to the standards of measurement, physiological interpretation and clinical use, as defined by the Task Force of The European Society of Cardiology and the North American Society of Pacing and Electrophysiology.[47] 10 five-minute samples of RR intervals were sampled within a six-hour window beginning the midnight after recording began. Ectopic beats, which may occur during the 48-hour period, were avoided by sampling areas where RR intervals were steady and consistent. This method of sampling has been shown to maximize stability and reproducibility of frequency-domain results. A frequency power spectrum was calculated for each five-minute sample using a built-in autoregressive (AR) feature, see Figure 5. Each spectrum is then separated into a very low frequency (VLF), low frequency (LF), and high-

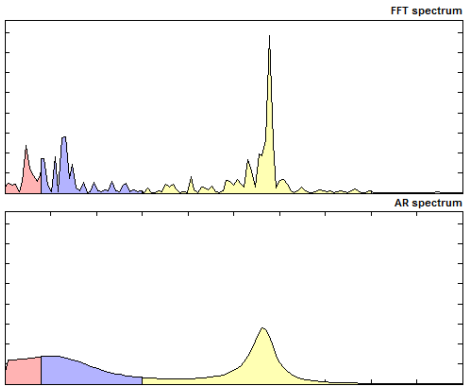

Figure 5. Kubios Spectrum Comparison. Fast Fourier transform (FFT) spectrum of RR interval sample (top) versus autoregressive (AR) spectrum of the same sample (bottom).

frequency (HF) component defined as 0-0.04 Hz, 0.04-0.15 Hz, and 0.15-0.4 Hz, respectively. The HF power in normalized units (n.u.) was calculated using Equation 6.

$$HF[n.u.] = \frac{HF[ms^2]}{total\ power\ [ms^2] - VLF[ms^2]}. \qquad \text{[Eq. 6]}$$

The median HF power across each of the ten samples was calculated and used as the primary metric for measuring the level of autonomic compensation in each DMD patient. This metric will be referred to as parasympathetic input-associated power (PIAP). An intraclass correlation coefficient was calculated in order to determine the reliability of the sampled time intervals for the HRV analysis. Each patient's 10 five-minute samples were randomly split into two groups. The PIAP values from these sample groups were then compared to assure that each set of ten samples were reliable data.

Statistical Analysis Defining Relationship between Variables

A Pearson coefficient and linear regression were also used to assess the correlation between ε_{cc} & PIAP, ε_{cc} & LVEF, ε_{cc} & age, and PIAP & age. Scatter plots provided visual representation of the data trends. Additionally, in order to assess the ability of PIAP values in predicting a less- versus more-severely diseased subject, patients were pooled in a "Healthy" and "Disease" category based on the following criteria.

	Table 1. Healthy vs Disease Separation Criteria	
	Healthy	Disease
LVEF	>60%	<55%
ε_{cc} Strain	>15%	<13%

Using LVEF and ε_{cc} as separate criteria, PIAP values from each category were compared using a Two-Sample t-Test assuming unequal variances. Patients were matched between groups according to their age and their use of β-blockers.

Chapter 3: Results

Filter Radius Optimization

Implementation of a GLM was used to assess the effect of varying harmonic peak filter radius (R_f) on calculated strain (ε_{cc}) values. The two iterations of the analysis produced similar results; the following reflects the results of using a single ε_{cc} set as a response variable. A visual representation of the GLM matrices can be seen in Figure 6. A fixed-effect analysis with R_f, LVEF, and age (in days) being the effect variables and each ε_{cc} set as the response variable showed that age and LVEF each had a statistically significant effect on ε_{cc} ($p<0.005$, $p<1.0\text{x}10^{-58}$, respectively). However, R_f did not have a significant effect on ε_{cc} ($p>0.25$). Next, a mixed-effect analysis was performed with the same effects and responses listed above, but with a patient identifier included as a random variable. Both R_f and LVEF had a statistically significant effect on ε_{cc} ($p<1.0\text{x}10^{-6}$, $p<0.005$, respectively), while age no longer had a significant p-value associated with ε_{cc} ($p>0.60$). The standard errors associated with the intercept, R_f, LVEF, and age were ~0.05, ~0.0001, ~0.008, and ~$3.0\text{x}10^{-6}$, respectively. The p-value associated with a constant intercept was non-significant

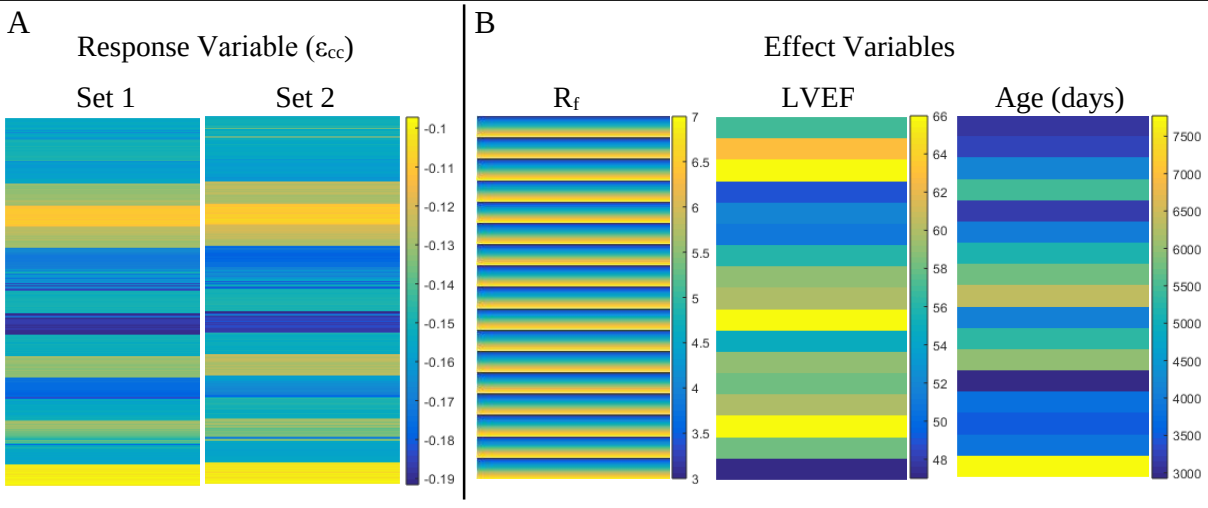

Figure 6. GLM Matrices Visualization. Visual representation of response variables y (A) and design matrix X (B). Each row represents a single run of the strain analysis algorithm on a patient with a given filter radius. A GLM was used to find parameters β such that $y = X\beta$.

for both the fixed- and mixed-analyses. Note that R_f became significantly associated with ε_{cc}, the LVEF-associated p-value increased many of orders of magnitude, and the age-associated p-value became insignificant when including patient ID as a random variable. The lower and upper boundaries of a 95% confidence interval of the effect of R_f (varied from 3-7 pixels) on ε_{cc} were ~ -0.001 and ~ -0.0005, respectively. Note that these values are small and clinically insignificant regarding disease characterization. This analysis shows that filter radius had a statistically significant effect on ε_{cc}, but a clinically insignificant effect on ε_{cc} magnitude. Further strain analysis was performed using an R_f value of 5 pixels. Again, the filter parameters were chosen to encompass spectral data corresponding to a maximum of ~30% strain magnitude.

Strain Analysis Validation

The results of the strain analysis algorithm developed were directly compared to the results produced from the same SPAMM-tagged images using a clinically trusted commercial HARP software. A scatterplot with the calculated strain values and the corresponding clinically used

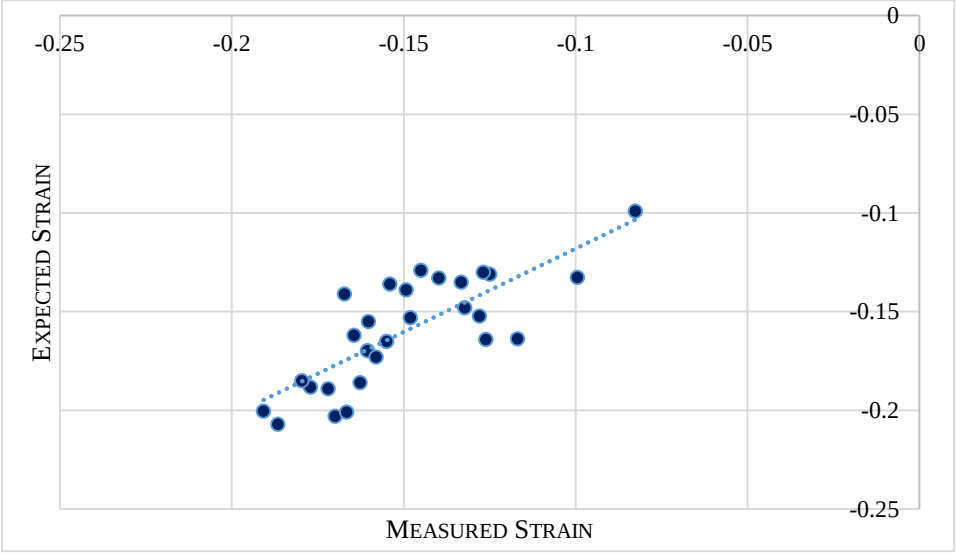

Figure 7. Strain Algorithm Comparison. Calculated strain values (horizontal axis) versus the corresponding clinically used strain values (vertical axis) for each patient.

strain values is displayed in Figure 7. From a simple linear regression, the two algorithms' results were seen to be significantly correlated ($p = 8.25 \times 10^{-7}$). Additionally, the correlation presented an R^2 value of 0.631 and a Pearson correlation coefficient of 0.783.

Example Strain Analysis Results & Patient Population Summary

Figures 8 and 9 each display results of the myocardial strain analysis that were compared to commercially-used HARP software. Figure 8 displays the results for a DMD patient with less severe cardiomyopathy, while Figure 9 displays results for a DMD patient with a more severe cardiomyopathy, as judged by their peak global strain ε_{cc}. The former and latter patients had a SPAMM sequence taken of a single cardiac cycle with 10 and 9 dynamics, respectively. According to these two figures, at dynamic 1, the heart is in a diastolic state, translating to a near-zero strain value. In later dynamics, the heart contracts and enters a systolic state, translating to more negative strain values. The heart then relaxes and reenters a diastolic state and strain values approach zero. Figure 8 strain values peak at ~ -17% while Figure 9 strain values peak at ~ -13%. Note that there are strain values of larger magnitude in dynamics towards the end of the SPAMM sequence while most of the heart is exhibiting lower-magnitude strain.

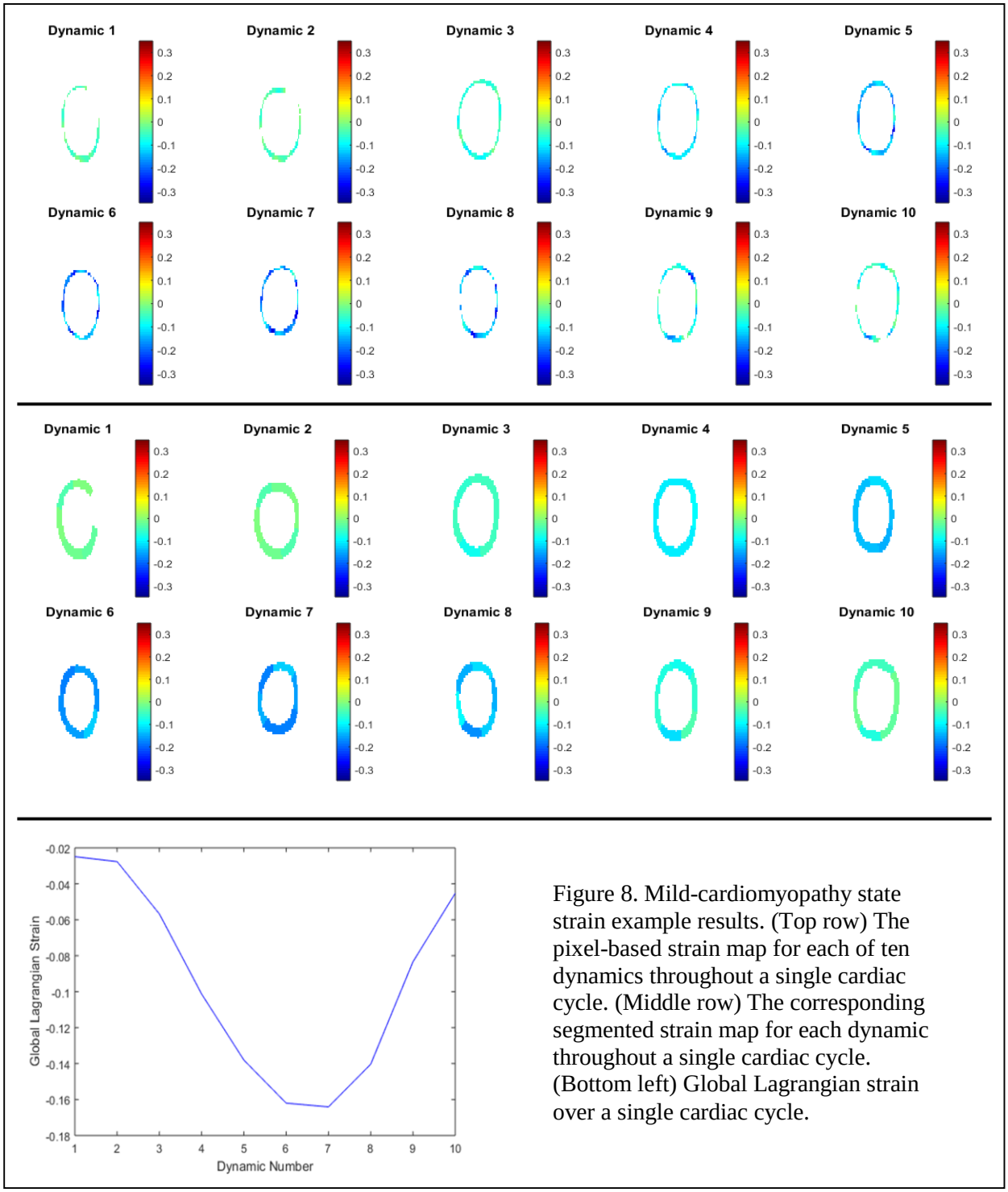

Figure 8. Mild-cardiomyopathy state strain example results. (Top row) The pixel-based strain map for each of ten dynamics throughout a single cardiac cycle. (Middle row) The corresponding segmented strain map for each dynamic throughout a single cardiac cycle. (Bottom left) Global Lagrangian strain over a single cardiac cycle.

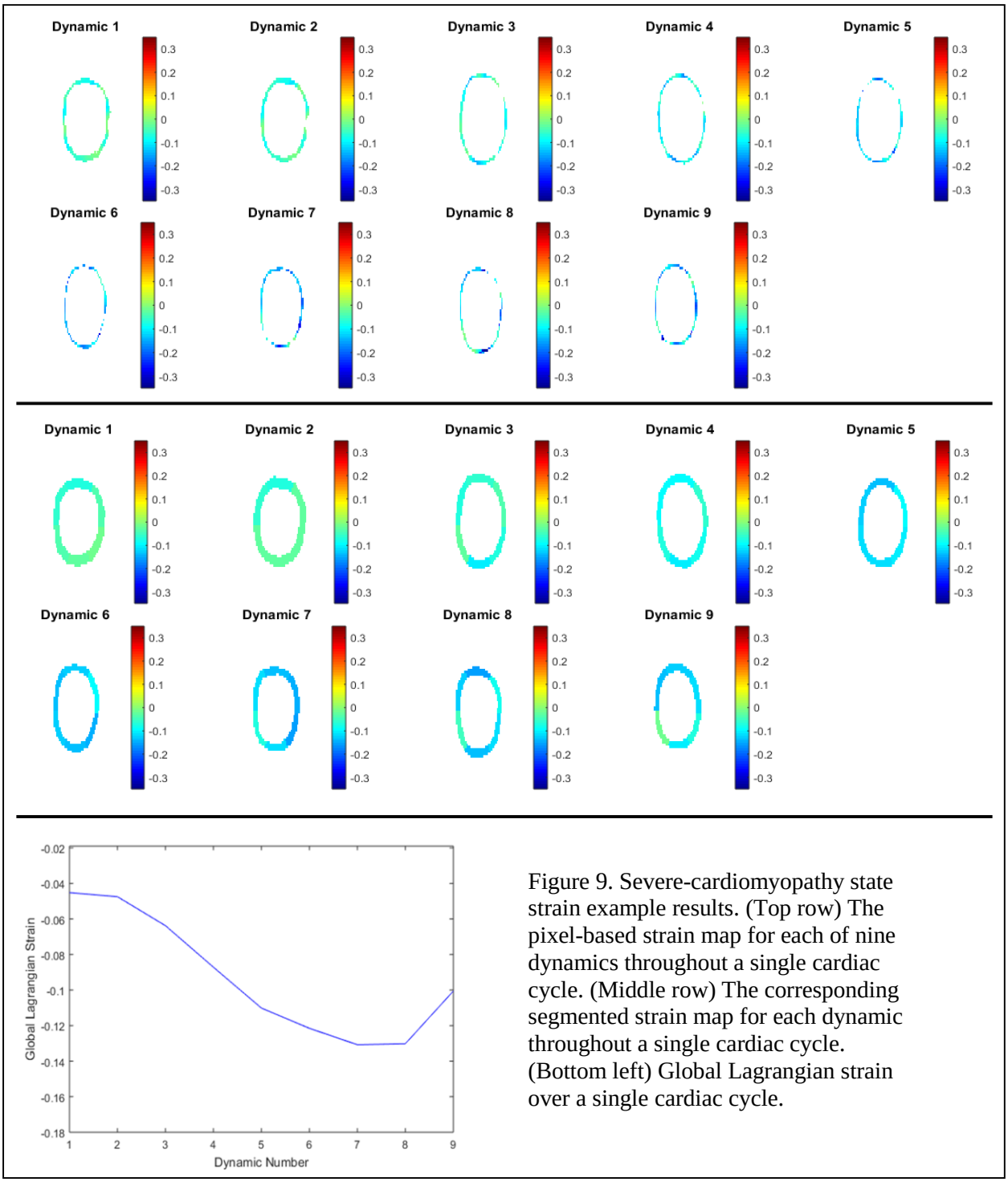

Figure 9. Severe-cardiomyopathy state strain example results. (Top row) The pixel-based strain map for each of nine dynamics throughout a single cardiac cycle. (Middle row) The corresponding segmented strain map for each dynamic throughout a single cardiac cycle. (Bottom left) Global Lagrangian strain over a single cardiac cycle.

Example Results of Heart Rate Variability Analysis

Figure 10 displays sample results from the Kubios HRV v2.1 software. Each set of spectra summarizes the power spectrum density of a five-minute sample taken within a six-hour window beginning at the midnight after application of the Holter monitor. The red, blue, and yellow portions of the spectrum represent the VLF, LF, and HF regions, respectively. Panel A shows data from a patient with less severe cardiomyopathy, while Panel B shows data from a patient with a more severe cardiomyopathy, as judged by their PIAP value. Though both FFT and AR spectra are seen here, the PIAP value extracted from each sample is from the AR analysis. The PIAP value from the above and below set are 73.3 n.u. and 27.8 n.u, respectively. These values reflect the percentage of power within the spectrum that falls under the HF range. It is deduced that this value

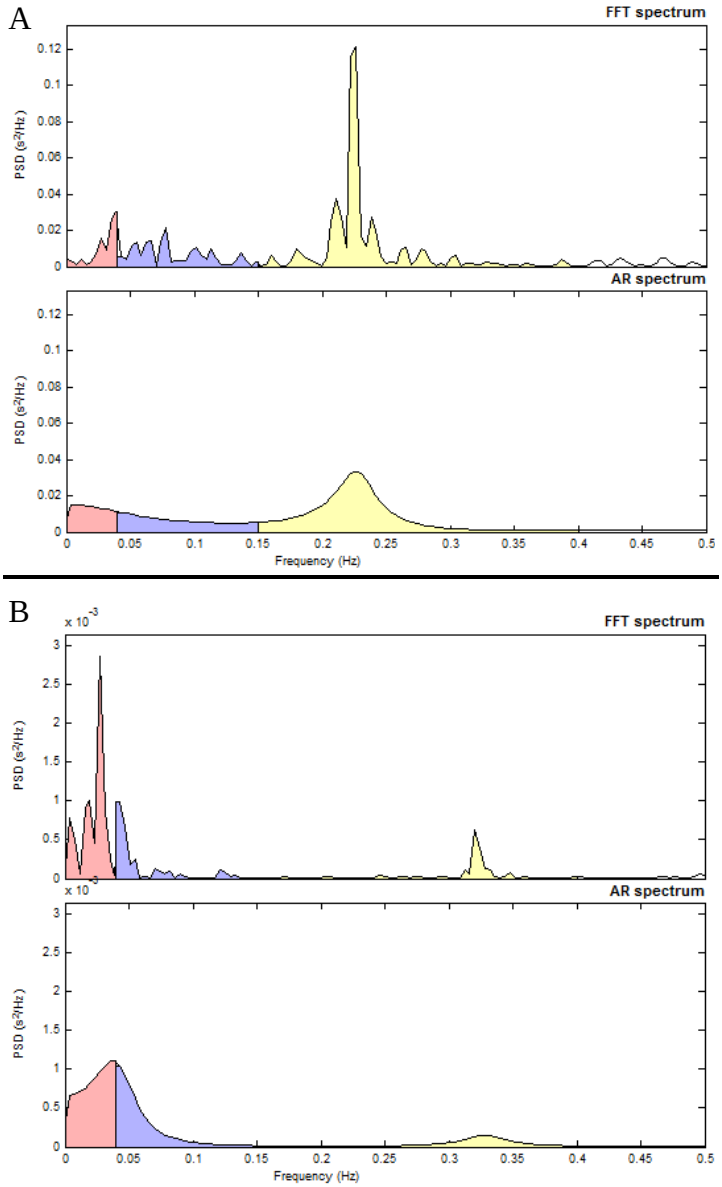

Figure 10. Comparison of HRV results between mild and severe cardiomyopathy patients. (A) FFT and AR power spectrum density (PSD) results from a patient with less-severe cardiomyopathy. (B) PSD results from patient with more-severe cardiomyopathy. See text for corresponding PIAP values.

also reflects the magnitude of parasympathetic input to the heart.

The PIAP measurements from the two randomly sampled periods of sleep did not differ significantly ($p=0.51$). Furthermore, an intraclass correlation of 0.923 ($p<0.001$; $n=28$) supported a high reliability of this data.

Patient Data Comparison

Figure 11 displays the comparison summary plots of all patients' data. The top left plot displays the measured peak global strain values versus the measured PIAP values. The two data sets were not significantly correlated (Pearson coefficient = -0.180, $p= 0.403$). This lack of statistical significance was consistent when excluding patients who were taking β-blockers at the time of the study (Pearson coefficient = -0.144, $p= 0.523$). The remaining Pearson coefficients and p-values for the other three relationships are summarized in Table 2.

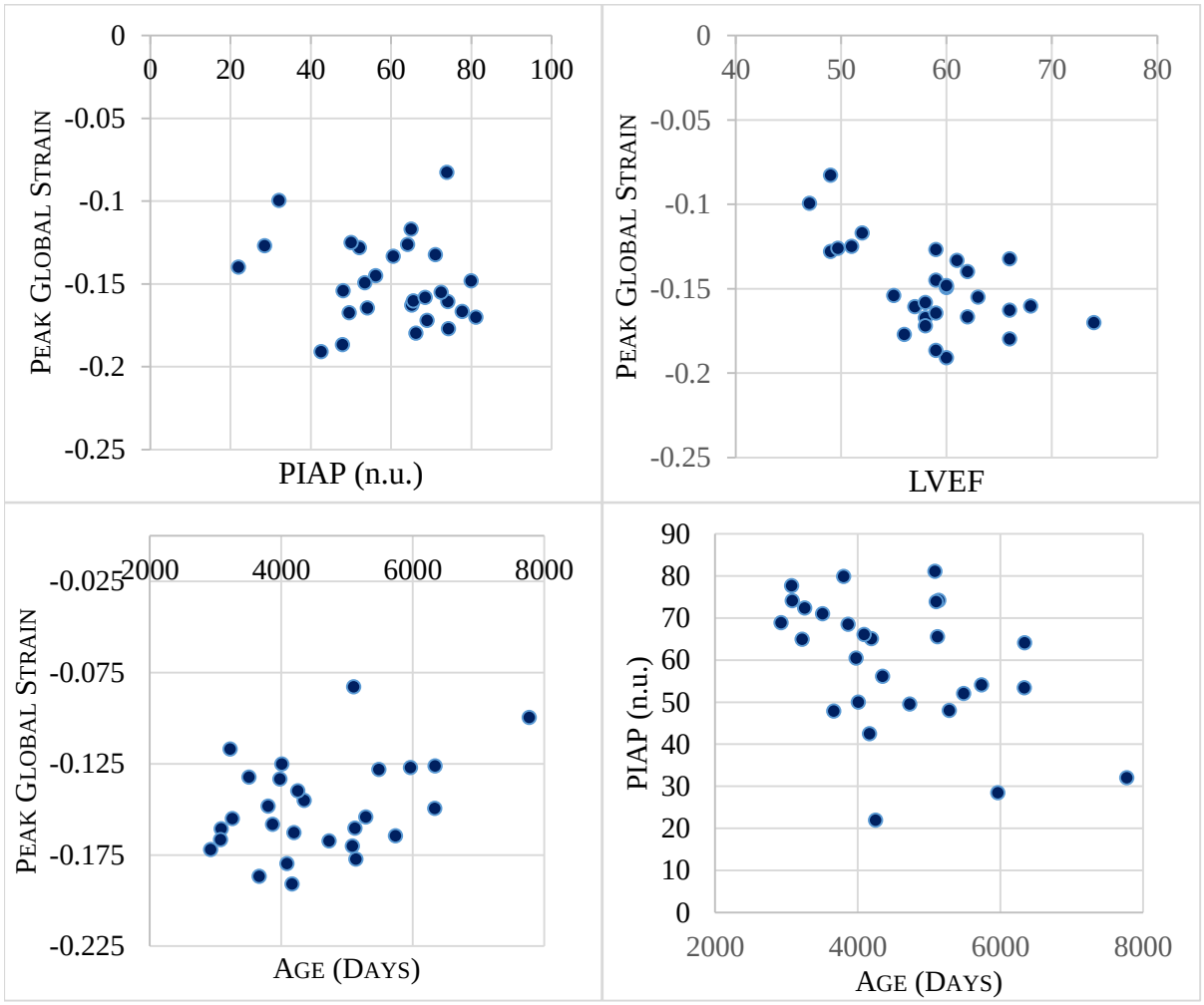

Figure 11. Data Comparison Summary Plots. (Top left) Peak global strain versus PIAP. (Top right) Peak global strain versus LVEF. (Bottom left) Peak global strain versus age in days. (Bottom right) PIAP versus age in days. These plots include patients who were taking β-blockers at the time of the study.

Table 2. Statistical Significance Summary of Variable Comparison

	Pearson Correlation Coefficient		Linear Regression P-value	
	Including βB	Excluding βB	Including βB	Excluding βB
ε_{cc} vs PIAP	-0.18	-0.14	0.40	0.52
ε_{cc} vs LVEF	-0.59	-0.56	8.8×10^{-4}	6.2×10^{-3}
ε_{cc} vs Age	0.37	0.38	0.051	0.077
PIAP vs Age	-0.45	-0.60	0.026	0.0033

Of the four comparisons, only "ε_{cc} vs LVEF" and "PIAP vs Age" were significantly correlated (both when including or excluding patients on β-blockers). Note that there was an increase in significance for "PIAP vs Age" when patients on β-blockers were excluded. Overall, excluding patients on β-blockers did not alter the relationships' significances.

A Two-Sample t-Test was used to assess the predictability of PIAP. PIAP did not differ significantly between patients with LVEF<55% and patients with LVEF>60% (n=5, p=0.16). Furthermore, PIAP did not differ significantly between patients with ε_{cc}<13% and patients with ε_{cc}>15% (n=5, p=0.093). Each of these separate groups were matched by age and β-blocker use. See Figure 12 for a visualization of these results.

Lastly, partial correlation analysis showed that PIAP decreased with age (r= -0.39, p<0.05) and that ε_{cc} and LVEF were significantly correlated (r= -0.54, p<0.005). However, PIAP was not correlated with LVEF or ε_{cc}.

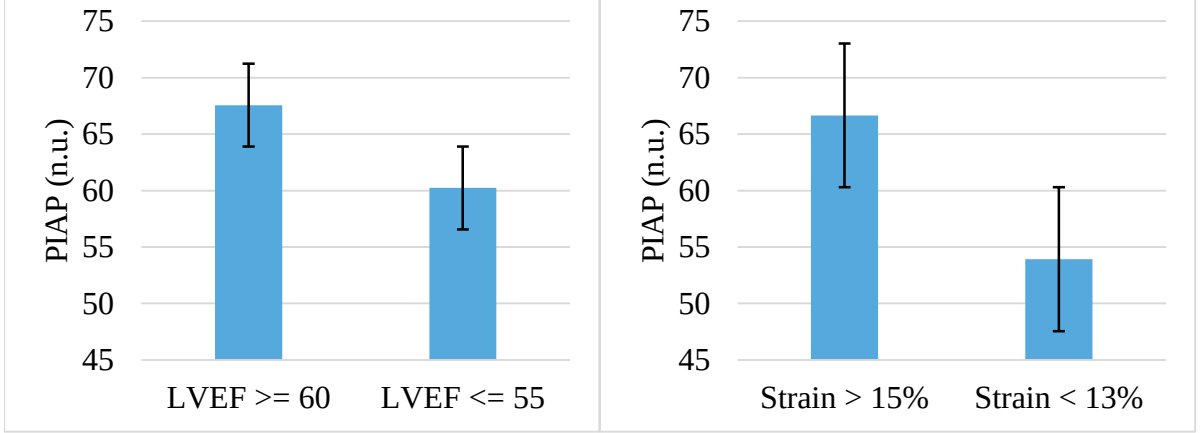

Figure 12. Assessment of PIAP in distinguishing less- and more- severe disease states. (Left) Patients were separated based on their LVEF values into a less-severe (LVEF>=60) and more-severe (LVEF<=55) cardiomyopathy states. (Right) Patients were separated based on their strain (ε_{cc}) values into a less-severe (Strain>15%) and more-severe (Strain<13%) cardiomyopathy states.

Chapter 4: Discussion

Myocardial Strain Analysis & Validation

Before the custom myocardial strain analysis algorithm results could be compared to HRV data, it was first validated by directly comparing the results to those of a clinically trusted commercial HARP software. Both analyses were performed on the identical SPAMM-tagged images for each of the 28 patients. The significant p-value ($p = 8.25x10^{-7}$) supports the hypothesis that the custom myocardial strain analysis is highly effective in calculating clinically relevant strain values in these patients. Furthermore, the physiologically accurate pattern in each strain result supported this conclusion. It remains, however, that thorough validation of this algorithm can only be done if it is directly compared to a gold standard measurement of myocardial circumferential strain (e.g. physical fiducial tracking in LV wall). However, determining significant correlation between the algorithm's results and those produced by a clinically-used software validates its clinical relevance within this patient sample.

As seen in Figures 8 and 9, the measured strain values begin and end at a near-zero value corresponding to the beginning and end diastolic states of the LV wall. The peak global circumferential strain magnitude occurs sometime between these two diastolic states, corresponding to the heart's peak systole. In order to achieve a spatial summary of strain values, each strain map from each SPAMM sequence was segmented into six LV wall segments (anterior, anteroseptal, inferoseptal, inferior, inferolateral, anterolateral). It can be expected that some segments would show lower peak strain magnitudes than others. These regions may correspond to regions of more severe cardiac tissue myopathy or higher fibrous tissue partial volume.

Furthermore, the significant correlation between strain and LVEF, both including and excluding patients on β-blockers, validated it as an accurate measure of cardiomyopathy. As stated

earlier, LVEF is classically considered a measure of cardiovascular disease; a significant correlation with the measured strain values supports the clinical relevance and potential of these values. In fact, studies continue to use LVEF not only as a measure of cardiomyopathy, but also as a standard to which developing detection methods are compared.[60, 61]

The bottom-up creation of a myocardial strain analysis method provided a flexible, adaptable framework for assessing cardiomyopathy in these patients. Due to proprietary reasons, further investigation into the commercial HARP software beyond its user interface was not an option. Therefore, constructing this algorithm with known parameters and relationships allowed for significantly increased transparency into the process of extracting strain values from the SPAMM-tagged images.

The implementation of Bayly et al.'s gradient-based analysis[46] of Osman et al.'s work on deformation gradient tensor construction[43] proved to be effective in measuring strain in this study. This expands the applicability of Bayly et al.'s method beyond mild traumatic brain injury patients and brain MR images and into, potentially numerous, dynamic cardiac applications.

Heart Rate Variability Analysis

The reliability of this analysis was validated by showing a lack of bias between two randomly sampled periods of sleep and a significant intraclass correlation coefficient. However, further validation and optimization of measuring PIAP would be appropriate. This includes optimizing the sampling method and parameters as well as the summary statistic selection.

As discussed earlier, studies have used both time-domain and frequency-domain parameters to assess the overall HRV in patients with DMD. According to the Task Force of the European Society of Cardiology and the North American Society of Pacing and Electrophysiology, the apparently easy derivation of HRV is what has popularized its use. In reality, the true

significance and meaning of the various measures of HRV are more complex than generally appreciated which leaves studies prone to incorrect conclusions and extrapolations.[4747] The shown reliability of PIAP supports the viability of using this measure as a specific, physiologically based metric of cardiac electrophysiology.

Relationship between HRV and Strain

To reiterate, we hypothesized that 1) the developed strain analysis technique would be correlated with the results achieved using commercialized HARP software, and 2) that the results seen would be significantly correlated with HRV parameters. Though this work supports the former portion of this hypothesis, the latter requires further research. The original relationship between strain and HRV was oriented around nervous system compensation in patients with DMD, resulting from a weakened cardiac state. At this point, we are unable to conclude that the strain values measured are significantly correlated to the magnitude of either sympathetic or parasympathetic input to the heart, as quantified by PIAP. After strain and PIAP were seen to have a nonsignificant relationship, they were each compared to patient age in order to compare their ability to predict disease severity within the studied age group. Due to the disease's progressive nature, DMD-associated cardiomyopathy is known to become more severe with age; data from healthy control subjects are needed to determine if this is a more significant relationship than what would be observed in a healthy population.

The two-sample t-test revealed that PIAP was an appreciable metric that distinguished the more- and less-severe disease states. Though the results are not statistically significant, we anticipate that a sample size greater than (n=5) would aid in decreasing the size of the measurement error and support PIAP as a promising method of distinguishing between varying severities of DMD cardiomyopathy.

Study Limitations: Strain Analysis

A major limitation of this study is that the circumferential strain measured was assumed to not contain any longitudinal component. In other words, the strain magnitudes measured only describe tissue displacement within the image slice plane. In reality, a longitudinal component would exist and contribute to the true physiological strain magnitude occurring within the LV. As this was a retrospective study, there was an inherent limitation to the accessibility of raw data, and so it was not possible to analyze multiple slices in the LV midsection to allow for 3-D strain estimation.

Additionally, segmentation of the LV wall via the MATLAB `roipoly` function introduced the possibility of user error by misclassifying LV wall tissue or including ancillary tissue regions such as the papillary muscle within the LV lumen. Using automatic segmentation algorithms allow for optimized classification of tissue and would significantly expedite the process of isolating the LV wall. However, the grid tag pattern on the SPAMM image prevents the use of automatic segmentation algorithms as various methods would mistake the grid line as a physiological tissue boundary; deciphering between non-smooth artificial signal changes and tissue signal changes can quickly become a complicated process to automate. Ideally, an untagged MR image within the same frame of reference and field of view taken concurrently to the SPAMM-tagged image would provide for a much easier image to use. This would allow researchers to use automatic segmentation methods such as seeding methods, K-means classification, or adaptive fuzzy C-means segmentation on the untagged images and register those to the tagged images to create a user input-free method of isolating the LV wall.

Another limitation to this study that affected the strain calculations was due to an inherent issue with SPAMM acquisition. Due to longitudinal relaxation, the contrast of the grid pattern

decreases tremendously from the beginning to the end of the SPAMM image sequence, as seen in Figure 13. This lack of signal of differentiation introduces image noise that varies throughout dynamics. This could alter the HARP algorithm's ability to extract relevant phase angle values pixel-to-pixel, introducing error into the strain measurements.

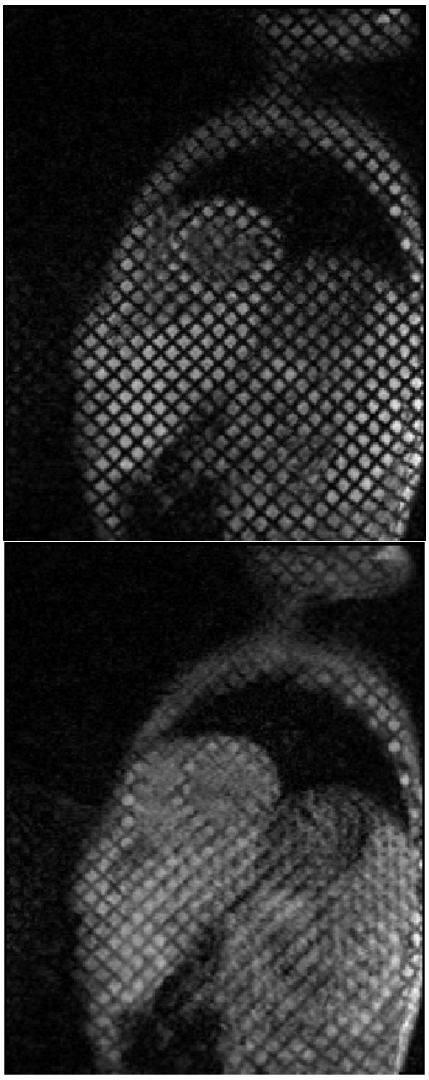

Figure 13. Effect of longitudinal relaxation on SPAMM-tagging contrast. (Top) First dynamic from a SPAMM sequence from beginning diastole. (Bottom) Last dynamic from same SPAMM sequence from end diastole.

Study Limitations: HRV Analysis

The lack of HRV data from control subjects prevented the determination of whether or not the observed relationship between PIAP and age was more significant than what would be observed in healthy individuals. Acquiring healthy control data would allow for this deciphering and could provide additional support towards PIAP being a reliable method of disease characterization.

Additionally, a major component of sampling R-R interval data, as done here, is to avoid sampling regions with ectopic heart beats, as these can significantly alter the resulting power density spectrum, depending on the length of the sampled region. Raw ECG data would be needed in order to locate and effectively avoid these abnormal HR regions. The Holter output data provided did not include the ECG signal of each patient, but only the R-R intervals. As the R-R intervals can be extracted from raw ECG data, collection of this raw data could provide increased accuracy for sampling.

Next Steps & Final Conclusions

Investigating the correlation between each of the six segments of the LV wall and PIAP values may reveal underlying significance between autonomic compensation and regional strain development. Regarding PIAP calculations, optimizing sampling parameters including sample duration and time of day could improve the validity and reproducibility of PIAP measurements. Furthermore, when separating patients into less- and more- severe disease states, stratifying patients based on ambulation would reduce any bias that could arise from an atrophied heart of a non-ambulatory patient.

The potential significance of this study remains promising. The validation of this HARP/strain analysis algorithm provides an alternate technique to quantifying Lagrangian LV strain in this patient population. Further optimization of this method can potentially aid in the development of improved pharmacological management and patient care regimen for patients with DMD. Furthermore, addressing the study limitations previously discussed can potentially define a significant correlation between LV circumferential strain and HRV parameters which would strengthen the argument that HR data can be utilized to provide clinically-relevant sequelae while omitting the need for resource-intensive, and often uncomfortable imaging techniques. Next steps of this study may also significantly improve the disease-state results discussed above and would support PIAP as a selective cardiomyopathy characterization metric. With further investigation, this work has the potential to directly impact both the treatment and quality of life in patients with Duchenne Muscular Dystrophy.

REFERENCES

1. Sienkiewicz, Dorota et al. “Duchenne Muscular Dystrophy: Current Cell Therapies.” Therapeutic advances in neurological disorders 8.4 (2015):166-177.

2. Braun, Robynne et al. Gene Therapy for Inherited Muscle Diseases: Where Genetics Meets Rehabilitation Medicine. American Journal of Physical Medicine & Rehabilitation 93 (2014): S97–S107.

3. Popov, S. G. et al. How Calcium Influx through Calcium Leak Channels Is Responsible for the Elevated Levels of Calcium-Dependent Proteolysis in Dystrophic Myotubes. Biol Chem 273 (1997): 17–749.

4. Blake, Derek J. et al. Function and Genetics of Dystrophin and Dystrophin-Related Proteins in Muscle. Physiological Reviews 82.2 (2002): 291–329.

5. Bushby, Katharine et al. Diagnosis and Management of Duchenne Muscular Dystrophy, Part 1: Diagnosis, and Pharmacological and Psychosocial Management. The Lancet Neurology 9.1 (2010): 77–93.

6. Bushby, Katharine et al.. Diagnosis and Management of Duchenne Muscular Dystrophy, Part 2: Implementation of Multidisciplinary Care. The Lancet Neurology 9.2 (2010): 177–189.

7. Aliverti, Andrea, Antonella LoMauro, and Maria Grazia D’Angelo. Assessment and Management of Respiratory Function in Patients with Duchenne Muscular Dystrophy: Current and Emerging Options. Therapeutics and Clinical Risk Management (2015): 1475.

8. Thomas, Tamara O. et al. Autonomic Dysfunction: A Driving Force for Myocardial Fibrosis in Young Duchenne Muscular Dystrophy Patients? Pediatric Cardiology 36.3 (2015): 561–568.

9. Kobinger, Gary P. et al. Correction of the Dystrophic Phenotype by in Vivo Targeting of Muscle Progenitor Cells. Human gene therapy 14.15 (2003): 1441–1449.

10. Konieczny, Patryk, Kristy Swiderski, and Jeffrey S. Chamberlain. Gene and Cell-Mediated Therapies for Muscular Dystrophy: Therapy for Muscular Dystrophy. Muscle & Nerve 47.5 (2013): 649–663.

11. Nowak, Kristen J., and Kay E. Davies. Duchenne Muscular Dystrophy and Dystrophin: Pathogenesis and Opportunities for Treatment. EMBO reports 5.9 (2004): 872–876.

12. Manzur, Adnan Y et al. Glucocorticoid Corticosteroids for Duchenne Muscular Dystrophy. Cochrane Database of Systematic Reviews. Ed. The Cochrane Collaboration. Chichester, UK: John Wiley & Sons, Ltd, (2008).

13. Angelini, Corrado, and Enrico Peterle. “Old and New Therapeutic Developments in Steroid Treatment in Duchenne Muscular Dystrophy.” Acta Myol 31.1 (2012): 9–15.

14. Raman, Subha V. et al. “Eplerenone for Early Cardiomyopathy in Duchenne Muscular Dystrophy: A Randomised, Double-Blind, Placebo-Controlled Trial.” The Lancet Neurology 14.2 (2015): 153–161.

15. “Vamorolone Will Advance to Phase 2 Testing for Treatment of DMD.” Muscular Dystrophy Association. March 2016.

16. Eagle, Michelle et al. Survival in Duchenne Muscular Dystrophy: Improvements in Life Expectancy since 1967 and the Impact of Home Nocturnal Ventilation. Neuromuscular disorders 12.10 (2002): 926–929.

17. Passamano, Luigia et al. Improvement of Survival in Duchenne Muscular Dystrophy: Retrospective Analysis of 835 Patients. Acta Myologica 31.2 (2012): 121.

18. Bach, J. R., and D. Martinez. “Duchenne Muscular Dystrophy: Continuous Noninvasive Ventilatory Support Prolongs Survival.” Respiratory Care 56.6 (2011): 744–750.

19. Wagner, Kathryn R., Noah Lechtzin, and Daniel P. Judge. “Current Treatment of Adult Duchenne Muscular Dystrophy.” Biochimica et Biophysica Acta (BBA) - Molecular Basis of Disease 1772.2 (2007): 229–237.

20. McNally, Elizabeth M. et al. Contemporary Cardiac Issues in Duchenne Muscular Dystrophy. Circulation 131.18 (2015): 1590–1598.

21. Judge, Daniel P. et al. Pathophysiology and Therapy of Cardiac Dysfunction in Duchenne Muscular Dystrophy. American Journal of Cardiovascular Drugs 11.5 (2011): 287–294.

22. Markham, L.W. et al. Steroid Therapy and Cardiac Function in Duchenne Muscular Dystrophy. Pediatric Cardiology 26.6 (2005): 768–771.

23. Duboc, Denis et al. Effect of Perindopril on the Onset and Progression of Left Ventricular Dysfunction in Duchenne Muscular Dystrophy. Journal of the American College of Cardiology 45.6 (2005): 855–857.

24. Matsumura, Tsuyoshi et al. Carvedilol Can Prevent Cardiac Events in Duchenne Muscular Dystrophy. Internal Medicine 49.14 (2010): 1357–1363.

25. Exner, Derek V. et al. Beta-Adrenergic Blocking Agent Use and Mortality in Patients With Asymptomatic and Symptomatic Left Ventricular Systolic Dysfunction: A Post Hoc Analysis of the Studies of Left Ventricular Dysfunction. Journal of American College of Cardiology 33.4 (1999): 916-923.

26. Baker, Jillian G, and Robert G Wilcox. β-Blockers, Heart Disease and COPD: Current Controversies and Uncertainties. Thorax (2016): 1-6.

27. Viollet, Laurence et al. Effects of Angiotensin-Converting Enzyme Inhibitors And/or Beta Blockers on the Cardiomyopathy in Duchenne Muscular Dystrophy. The American Journal of Cardiology 110.1 (2012): 98–102.

28. Posner, Andrew D et al. The Correlation of Skeletal and Cardiac Muscle Dysfunction in Duchenne Muscular Dystrophy. Journal of Neuromuscular Diseases 3.1 (2016): 91–99.

29. de Kermadec, Jean-Michael et al. Prevalence of Left Ventricular Systolic Dysfunction in Duchenne Muscular Dystrophy: An Echocardiographic Study. American Heart Journal 127.3 (1994): 618–623.

30. Danilowicz, Delores et al. Echocardiography in Duchenne Muscular Dystrophy. Muscle & Nerve 3 (1980): 298–303.

31. Jefferies, J. L. Genetic Predictors and Remodeling of Dilated Cardiomyopathy in Muscular Dystrophy. Circulation 112.18 (2005): 2799–2804.

32. Hor, Kan N. et al. Circumferential Strain Analysis Identifies Strata of Cardiomyopathy in Duchenne Muscular Dystrophy. Journal of the American College of Cardiology 53.14 (2009): 1204–1210.

33. Silva, Marly Conceição et al. Myocardial Delayed Enhancement by Magnetic Resonance Imaging in Patients With Muscular Dystrophy. Journal of the American College of Cardiology 49.18 (2007): 1874–1879.

34. Yilmaz, Ali et al. Cardiac Involvement in Patients with Becker Muscular Dystrophy: New Diagnostic and Pathophysiological Insights by a CMR Approach. Journal of Cardiovascular Magnetic Resonance 10.1 (2008): 50.

35. Soslow, Jonathan H et al. Left Ventricular Function by Echocardiography Correlates Poorly with Cardiac MRI Measures in Duchenne Muscular Dystrophy. Journal of Cardiovascular Magnetic Resonance 16.Suppl 1 (2014): P306.

36. Smith, Gillian et al. Primary Myocardial Dysfunction in Autosomal Dominant EDMD. A Tissue Doppler and Cardiovascular Magnetic Resonance Study. Journal of Cardiovascular Magnetic Resonance 8.5 (2006): 723–730.

37. Axel, Leon, and Lawrence Dougherty. Heart Wall Motion: Improved Method of Spatial Modulation of Magnetization for MR Imaging. Cardiac Radiology 172 (1989): 349–350.

38. Connor, S.E.J. et al. SPAMM, Cine Phase Contrast Imaging and Fast Spin-Echo T2-Weighted Imaging in the Study of Intracranial Cerebrospinal Fluid (CSF) Flow. Clinical Radiology 56.9 (2001): 763–772.

39. Sugimori, Hiroyuki et al. Comparison of SPAMM and SENC Methods for Evaluating Peak Circumferential Strain at 3T. Magnetic Resonance in Medical Sciences 12.1 (2013): 69–75.

40. Ashford, M.W. Occult Cardiac Contractile Dysfunction in Dystrophin-Deficient Children Revealed by Cardiac Magnetic Resonance Strain Imaging. Circulation 112.16 (2005): 2462–2467.

41. Hagenbuch, Sean C. et al. Detection of Progressive Cardiac Dysfunction by Serial Evaluation of Circumferential Strain in Patients with Duchenne Muscular Dystrophy. The American Journal of Cardiology 105.10 (2010): 1451–1455.

42. Revel, Didier, and David A. Bluemke. Cardiac Magnetic Resonance. Diseases of the Chest and Heart 2015–2018. Ed. J. Hodler et al. Milano: Springer Milan, 2015. 134–142.

43. Osman, Nael F. et al. Cardiac Motion Tracking Using CINE Harmonic Phase (HARP) Magnetic Resonance Imaging. Magnetic resonance in medicine: official journal of the Society of Magnetic Resonance in Medicine/Society of Magnetic Resonance in Medicine 42.6 (1999): 1048.

44. Osman, Nael F., Elliot R. McVeigh, and Jerry L. Prince. Imaging Heart Motion Using Harmonic Phase MRI. IEEE transactions on medical imaging 19.3 (2000): 186–202.

45. Osman, N.F., and J.L. Prince. Regenerating MR Tagged Images Using Harmonic Phase (HARP) Methods. IEEE Transactions on Biomedical Engineering 51.8 (2004): 1428–1433.

46. Bayly, P. V. Measurement of Strain in Physical Models of Brain Injury: A Method Based on HARP Analysis of Tagged Magnetic Resonance Images (MRI). Journal of Biomechanical Engineering 126.4 (2004): 523.

47. Task Force of the European Society of Cardiology and the North American Society of Pacing and Electrophysiology. Heart Rate Variability: Standards of Measurement, Physiological Interpretation and Clinical Use. Circulation 17 (1996): 354–381.

48. Dhargave, Pradnya et al. Assessment of Cardiac Autonomic Function in Patients with Duchenne Muscular Dystrophy Using Short Term Heart Rate Variability Measures. European Journal of Paediatric Neurology 18.3 (2014): 317–320.

49. Dittrich, S. et al. Cardiomyopathy in Duchenne Muscular Dystrophy: Current Value of Clinical, Electrophysiological and Imaging Findings in Children and Teenagers. Klinische Pädiatrie 227.04 (2015): 225–231.

50. De Jong, Maj Marla J., and David C. Randall. Heart Rate Variability Analysis in the Assessment of Autonomic Function in Heart Failure. Journal of Cardiovascular Nursing 20.3 (2005): 186–195.

51. Lahiri, Marc K., Prince J. Kannankeril, and Jeffrey J. Goldberger. Assessment of Autonomic Function in Cardiovascular Disease. Journal of the American College of Cardiology 51.18 (2008): 1725–1733.

52. Tarvainen, Mika P. et al. “Kubios HRV – Heart Rate Variability Analysis Software.” Computer Methods and Programs in Biomedicine 113.1 (2014): 210–220.

53. Malliani, Alberto et al. Cardiovascular Neural Regulation Explored in the Frequency Domain. Circulation 84.2 (1991): 482–492.

54. Malik, Marek, and A. John Camm. Components of Heart Rate Variability—what They Really Mean and What We Really Measure. The American journal of cardiology 72.11 (1993): 821–822.

55. Malliani, Alberto et al. The Pattern of Sympathovagal Balance Explored in the Frequency Domain. Physiology 14.3 (1999): 111–117.

56. Niemelä, Matti J., KE Juhani Airaksinen, and Heikki V. Huikuri. Effect of Beta-Blockade on Heart Rate Variability in Patients with Coronary Artery Disease. Journal of the American College of Cardiology 23.6 (1994): 1370–1377.

57. Aronson, Doron, and Andrew J. Burger. Effect of Beta-Blockade on Heart Rate Variability in Decompensated Heart Failure. International journal of cardiology 79.1 (2001): 31–39.

58. Wansapura, Janaka P. et al. "Left Ventricular T2 Distribution in Duchenne Muscular Dystrophy." Journal of Cardiovascular Magnetic Resonance 12.1 (2010): 14.

59. Smit, Carey, Spottiswoode, Bruce (2010) GolsteinUnwrap2D_r1. <www.mathworks.com/matlabcentral/fileexchange/29497-goldsteinunwrap2d-r1>.

60. Fayssoil, Abdallah, Soumeth Abasse, and Katy Silverston. "Cardiac Involvement Classification and Therapeutic Management in Patients with Duchenne Muscular Dystrophy." Journal of Neuromuscular Diseases 4.1 (2017): 17–23.

61. Silva, Marly Conceição et al. "Myocardial Fibrosis Progression in Duchenne and Becker Muscular Dystrophy: A Randomized Clinical Trial." JAMA Cardiology 2.2 (2017): 190.